Low-Sidelobe Dual-Beam Antenna Based on Metasurface With Independently Regulated Amplitude/Phase

Pengfei Zhang, Wenmei Zhang, *Senior Member, IEEE*, Xinwei Chen, Guorui Han, Jinrong Su, and Rongcao Yang

***Abstract*—A method to design low-sidelobe dual-beam antennas is proposed based on metasurface with independently regulated amplitude/phase. This method includes the following steps. First, a standard horn antenna is modeled and the amplitude and phase of the radiation field at the interface are obtained. Next, the phase compensation technology based on the actual radiation phase of the feed is employed to control directions of the main lobe. Finally, the reflection amplitude of metasurface is controlled by combining Schelkunoff polynomials and actual radiation amplitude of the feed. Specifically, by mapping the angles of the dual beams to the complex coordinate system, the sidelobe level of the dual-beam antenna is reduced. Meanwhile, a compensation factor is introduced to offset the gain loss caused by amplitude modulation.**

***Index Terms*—Dual beam, metasurface, phase- and amplitude-control, Schelkunoff polynomial method, sidelobe suppression.**

I. Introduction

In RECENT years, many transmissive [1], [2] and reflective [3], [4] array antennas based on metasurfaces have been proposed. Moreover, some researchers have figured out ways to reduce sidelobe of single beam antennas [5], [6]. Li et al. [5] designed an antenna with a Taylor amplitude-distribution metasurface and successfully reduced the SLLs. In [6], two metasurfaces with controllable amplitude and phase were designed respectively to suppress the SLLs.

Compared with single-beam antennas, multibeam antennas have more advantages in some specific scenarios, such as microwave energy transmission and multitarget radar detection [7]. Moreover, multibeam antennas are considered as the key technology of the fifth-generation (5G) wireless communication network and have been used in point-to-multipoint and multipoint-to-multipoint communications [8], [9], [10]. With the emergence of metasurface, theories related to multibeam antennas based on metasurface have also been studied [11], [12], [13], which have been widely applied to many aspects, such as multibeam scanning antennas [14], multibeam near-field focusing antennas [15], and multibeam lens antennas [16]. Lee et al. [11] realized a four-beam circularly polarized antenna based on a transmissive metasurface using equivalent circuit model and superposition principle. Three single-feed and quad-beam reflectarray antennas were proposed by Nayeri et al. [13] using geometrical, superposition and alternating projection methods, respectively [13]. In [14], a folded reflectarray antenna composed of three different metasurfaces was proposed to realize a scanning range of 60°.

So far, many excellent works have been achieved in multibeam antennas based on metasurface. But it is found that conventional methods of suppressing the SLLs, such as those based on Chebyshev and Taylor distributions, are mainly used for single beam case. Up to now, few of works involve the suppression of SLLs for multibeam antennas.

In this letter, based on the metasurface which has independently control amplitude and phase, we propose a design method of dual-beam antennas with low SLLs. Main points of this method include the following aspects. First, when compensating the phases of metasurface, the actual radiation phase of the feed is considered. Second one is that the amplitude modulation combining the Schelkunoff polynomials and the actual radiation field of the feed is carried out. Specifically, by mapping the beam angles to the complex coordinate system and adjusting distributions of roots on the unit circle, the amplitude distribution over the aperture to achieve low SLL is obtained. In addition, a compensation factor γ is introduced to offset the gain loss caused by amplitude modulation.

II. Dual-Beam Antenna Based on Phase-Regulated Metasurface

In this section, the dual-beam antenna MS_0 based on the phase regulation is designed. Here, phase compensation technology is based on the actual radiation phase of the feed.

A. *Phase Compensation Technology Based on the Actual Radiation Phase of the Feed*

Generally, the phase compensation is based on the spherical wave's formula [4]. Here, another technology based on the actual radiation phase of the feed is introduced. The main points of the method are as follows. First, simulate the feed and obtain the phase ph_{mn} of the feed at the metasurface position. Then, calculate the compensated phase $\Delta\phi_{\mathrm{mn}}$ for single beam according

Manuscript received 7 May 2023; accepted 16 June 2023. Date of publication 22 June 2023; date of current version 6 October 2023. This work was supported in part by the National Science Foundation of China under Grant 62071282, and in part by the National Science Foundation of Shanxi Province under Grant 202203021211295. *(Corresponding author: Wenmei Zhang.)*

The authors are with the School of Physics and Electronic Engineering, Shanxi University, Shanxi 030006, China (e-mail: 1595040095@qq.com; zhangwm@sxu.edu.cn; chenxw@sxu.edu.cn; han_gr@sxu.edu.cn; sujinrong@sxu.edu.cn; sxdxyrc@sxu.edu.cn).

Digital Object Identifier 10.1109/LAWP.2023.3288601

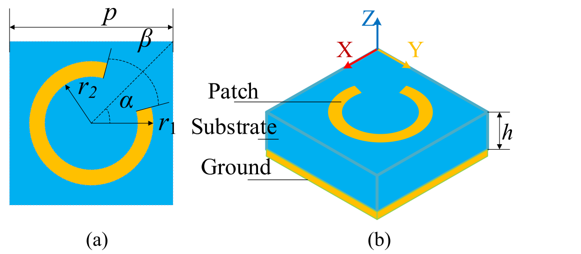

Fig. 1. Structure of the C-shaped particle. (a) Top view. (b) Perspective view.

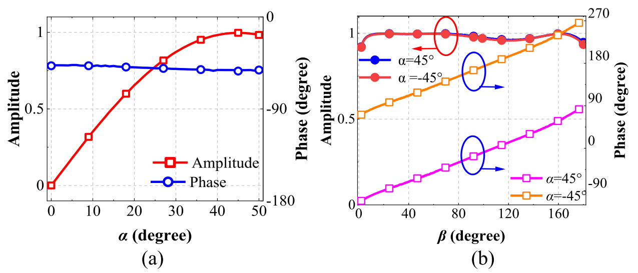

Fig. 2. Amplitude and phase responses of the unit at 16 GHz. (a) $\beta = 60°$, α is different. (b) β is different.

to

$$\Delta\phi_{\mathrm{mn}} = -ph_{\mathrm{mn}} - \frac{2\pi}{\lambda 0}(m \times \sin\theta\cos\varphi + n \times \sin\theta\sin\varphi) \pm 2k\pi \quad (1)$$

where λ_0 is the wavelength of electromagnetic waves in vacuum, m and n are the index numbers of the unit on x-axis and y-axis respectively, θ and φ are the elevation and azimuth angle of the beam, respectively.

For dual-beam antennas, the phase of each element can be obtained according to superposition method [13]. Assuming that the two beams point to (θ_1, φ_1) and (θ_2,φ_2), respectively, then, the phase $\Delta\phi_{\mathrm{mn}}^{\mathrm{final}}$ for each element on the metasurface is

$$\Delta\phi_{\mathrm{mn}}^{\mathrm{final}} = Arg\left(e^{j\Delta\phi_{\mathrm{mn}}^{1}} + e^{j\Delta\phi_{\mathrm{mn}}^{2}}\right). \quad (2)$$

B. Design Example

Here, the C-shaped particle (shown in Fig. 1) whose reflection amplitude and phase can be regulated independently is selected to form the metasurface [12]. It is printed on the F_4BM265 dielectric ($\varepsilon = 2.65$, tan$\delta = 0.0015$, $h = 2$ mm, $p = 5$ mm, $r_1 = 2$ mm, and $r_2 = 1.5$ mm) with a ground plane and has a rotation angle α (with respect to the x-axis) and an opening angle β. The C-shaped particle is simulated using the CST Microwave Studio and the results at 16 GHz are shown in Fig. 2. Here, the incident and reflected waves are y- and x-polarized wave, respectively. In Fig. 2(a), when β is fixed at 60°, the reflection amplitude of the unit can be linearly changed from 0 to 1 by adjusting α, while the variation of reflection phases is less than 10°. In Fig. 2(b), when $\alpha = 45°$, the reflection phase increases from $-115.7°$ to 82.67° with β. When $\alpha = -45°$, the corresponding phase increases from 67.03° to 265.7°. That is, the overall phase covers the range of 381.4°. Also, the reflection amplitude keeps around 1.

A standard horn LB-62-10-C-SF from A-INFO is used as a central feed. It is placed 90 mm (0.85D, D is the size of aperture) above the metasurface to achieve high aperture efficiency (η_{a}). To get an overview of η_{a}, the radiation patterns of the feeder and element are modeled first by "$\cos^{2q}(\theta)$" and "$\cos^{2qe}(\theta)$," and the value of "q" and "qe" can be regarded as 4.25 and 1, respectively. Then, η_{a} derived by the spillover efficiency and illumination efficiency [17] is 65.8%. The radiation amplitude I and phase distribution Ph_{mn} in this position are shown in Fig. 3.

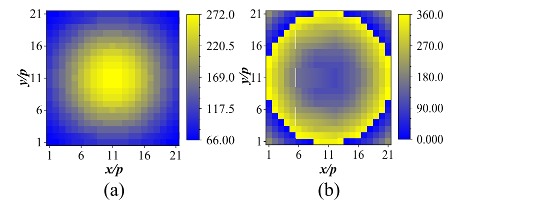

Fig. 3. Distribution of radiation field 90 mm above the feed at 16 GHz. (a) I. (b) Ph_{mn}.

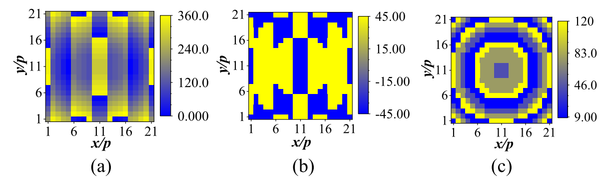

Fig. 4. Distribution of (a) $\Delta\phi_{\mathrm{mn}}^{\mathrm{final}}$, (b) α, and (c) β.

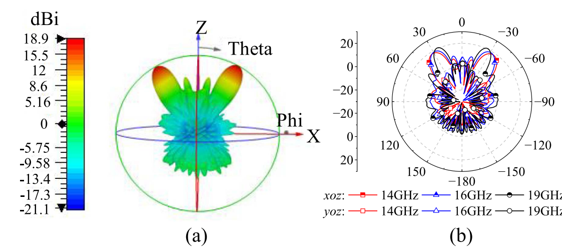

Fig. 5. Simulated radiation pattern of MS_0. (a) 3-D result at 16 GHz. (b) 2-D results in xoz-and yoz-plane.

According to the superposition principle, we design a dual-beam antenna MS_0 with the beams pointing to (θ_1, φ_1) = (30°, 0°) and (θ_2, φ_2) = (30°, 180°). According to Fig. 3(b) and (1) and (2), the phase $\Delta\phi_{\mathrm{mn}}^{\mathrm{final}}$ can be obtained and shown in Fig. 4(a). Further, α and β of the C-shaped particle are shown in Fig. 4(b) and (c). Fig. 5 shows typical results of MS_0. At 14, 16, and 19 GHz, MS_0 has gains of 17.6, 18.9, and 19.4 dBi, SLLs of -11.2, -9.2, and -12.9 dB in the xoz plane and -12.6, -12.1, and -12.98 dB in the yoz plane. Also, the main beams point to $\theta = \pm 31°$, $\pm 30°$ and $\pm 28°$, respectively.

III. Dual-Beam Antenna Introducing Amplitude Modulation

In the previous section, the dual-beam antenna MS_0 based on the phase regulation has high SLLs. In this section, based on MS_0, we will further adopt the Schelkunoff polynomial method to regulate the reflection amplitude and suppress the SLLs.

A. Amplitude Control Method Based on Schelkunoff Polynomial

Schelkunoff Polynomial Method [18] is the basic method of sidelobe optimization in traditional array antenna synthesis.

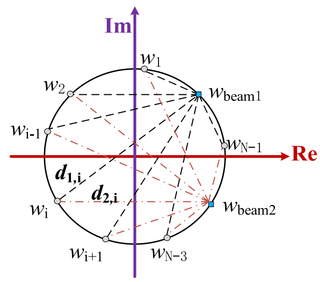

Fig. 6. Roots distribution of an *N*-element linear array.

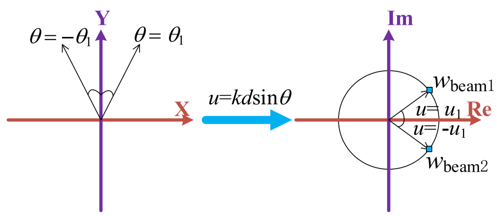

Fig. 7. Schematic of coordinate transformation.

Here, based on it, a new method to suppress the SLLs of dual-beam antennas is proposed.

For an N-element symmetric linear array, the magnitude of its array factor polynomial $S(w)$ can be expressed as

$$|S(w)| = \prod_{n=1}^{N-1} |(w - w_{\text{n}})| \tag{3}$$

$$w = e^{ju} \tag{4}$$

$$u = kd \sin\theta \tag{5}$$

where $w_1, w_2, \ldots, w_n$ are the roots of the polynomial, and u is the phase angle of the root on the unit circle, $k = 2\pi/\lambda$, d is the distance between two adjacent elements. According to the Schelkunoff Polynomial Method, the maximum lobe generally appears at the center position between two adjacent roots. For example, as shown in Fig. 6, if the distance from w_{beam1} to all zeros are $d_{1,1}, \ldots, d_{1,\text{i}}, \ldots, d_{1,\text{N}-1}$, respectively, the level of the main lobe S_{beam1} can be calculated by

$$\begin{aligned} S_{\text{beam}} &= \prod_{n=1}^{N-1} |(w_{\text{beam}} - w_{\text{n}})| \\ &= d_{1,1} \times \ldots \times d_{1,\text{i}} \ldots \times d_{1,\text{N}-1}. \end{aligned} \tag{6}$$

The level of the other lobes S_{i} can also be obtained as follows:

$$S_{\text{i}} = \prod_{n=1}^{N-1} |((w_{\text{i}} + w_{\text{i+1}})/2 - w_{\text{n}})|. \tag{7}$$

Finally, the sidelobe level Sll_{i} is obtained as

$$Sll_{\text{i}} = 20\lg|S_{\text{i}}/S_{\text{beam}}|. \tag{8}$$

Once the roots, $w_1, w_2, \ldots, w_n$ are determined, the Schelkunoff-amplitude of the unit cells can be obtained by (3). In the following section, we will show how to determine the position of roots on the circle (take the roots on the upper semicircle for example). First, as is shown in the Fig. 7, (5) is used to transform the angle $\pm\theta_1$ (in the Cartesian coordinate system) into $\pm u_1$ (in the complex plane coordinate system). Then, take w_{beam1} as the center to arrange w_1 and $w_{\text{N-1}}$. The rest w_{i} are evenly distributed in the remaining space of the upper semicircle. After that, an optimization program in Mathematica is used to find these roots. The basic optimization criterion is that the closer two adjacent roots w_{i} and $w_{\text{i+1}}$ are, the lower the relative level of the lobe will be. For example, if Sll_1 calculated by (7) and (8) is higher than the target value, the space between w_1 and $w_{\text{N-1}}$ is increased. If Sll_1 is lower than the target value, but the other Sll_{i} is higher than the target value, the space between w_{i} and $w_{\text{i+1}}$ is reduced.

TABLE I
Excitation Distribution of MS_1

Unit number	1/21	2/20	3/19	4/18	5/17	6/16
A_0	1	0.023	0.517	1.582	0.797	0.087
A_1	0.406	0.009	0.21	0.643	0.324	0.035
Unit number	**7/15**	**8/14**	**9/13**	**10/12**	**11**	
A_0	2.241	2.043	0.8	1.951	2.461	
A_1	0.91	0.83	0.325	0.793	1	

B. Design Example

To verify the feasibility of the proposed method, amplitude modulation is added based on MS_0, and the corresponding antenna is denoted as MS_1. Considering that the lower the SLL is, the wider the beamwidth becomes, the target SLL at 16 GHz is set to -30 dB, and SLLs in the whole operating band are set less than -20 dB. After optimization, the position of the roots on the unit circle are determined, which are $\pm7°$, $\pm17°$, $\pm25°$, $\pm75°$, $\pm85°$, $\pm100°$, $\pm120°$, $\pm135°$, $\pm150°$, and $\pm165°$. Substituting these roots into (3), we can get a polynomial about $S(w)$, in which coefficients of the polynomial represent the relative reflection amplitude of the elements, namely "A_0." Considering the realizability for the C-shaped particle, the Schelkunoff amplitude A_0 is normalized and denoted as a row vector "A_1" (a matrix of 1×21), and the corresponding results are listed in Table I. Then, the matrix of reflective amplitude of the unit cells "T_{x}" can be obtained as

$$T_x(m,n) = \{[A_2(m,1) \times A_1(1,n)] \,/\, [I(m,n)/I(m,11)]\} \times \gamma \tag{9}$$

where "A_2" is a 21×1 column vector of all "1," which is used to transform Schelkunoff amplitude from 1-D into 2-D aperture. "$I(m, n)/I(m,11)$" is the normalized feed's amplitude (shown in Fig. 3). The mechanism of the (9) is that "I" is converted into "A" by "T_{x}," that is "$I \times T_x = A$". Therefore, "$T_x = A/I$." "γ" is the compensation factor, which is larger than 1 to offset the gain loss caused by amplitude modulation. It should be noted that some of T_{x} will be larger than 1 after multiplied by "γ." In this case, these T_{x} need setting to be 1, which is the maximum value for the reflected unit cells. With the increase of γ, more T_{x} will deviate from original value for $\gamma = 1$ and lead to increase of SLLs. Table II lists T_{x} while γ is 1.2 and 1.3. It can be seen, when $\gamma = 1.2$, there are three amplitudes larger than 1. But as $\gamma = 1.3$, the numbers larger than 1 increase to 7. After comparison, $\gamma = 1.2$ is selected and the distribution of T_{x} and α are shown in Fig. 8.

The simulated results of MS_1 are shown in Fig. 9. At 14, 16, and 19 GHz, MS_1 has gains of 18.2, 19.1, and 20.1 dBi, SLLs of -21.67, -30.4, and -21.23 dB in the *xoz*-plane and SLLs of -17.2, -18.98, and -19.6 dB in the *yoz*-plane. Table III lists results of comparison, which show that the SLLs of MS_1 are

TABLE II
DISTRIBUTION OF T_x WHILE γ IS 1.2 AND 1.3

Unit number	1/21	2/20	3/19	4/18	5/17	6/16
γ=1.2	0.487	0.011	0.252	0.772	0.389	0.042
γ=1.3	0.528	0.012	0.273	0.836	0.421	0.046
Unit number	**7/15**	**8/14**	**9/13**	**10/12**	**11**	
γ=1.2	1.092	0.996	0.39	0.952	1.2	
γ=1.3	1.183	1.079	0.423	1.031	1.3	

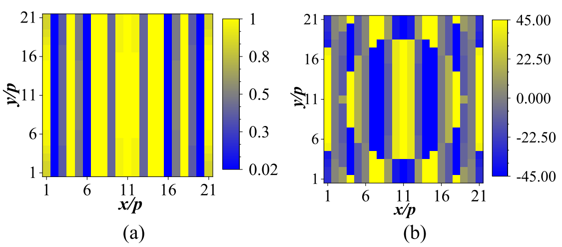

Fig. 8. Distribution of (a) T_x matrix and (b) α matrix when $\gamma = 1.2$ of MS_1.

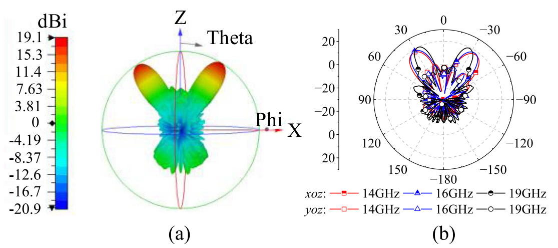

Fig. 9. Simulated radiation patterns of MS_1. (a) 3-D result at 16 GHz. (b) 2-D results in *xoz*-and *yoz*-plane.

TABLE III
COMPARISON RESULTS AT DIFFERENT FREQUENCIES OF MS_0 AND MS_1

		14GHz	16GHz	19GHz
MS_0	Gain(dBi)	17.6	18.9	19.4
	SLL (dB) (*xoz*/*yoz*)	-11.2/-12.6	-9.2/-12.1	-12.9/-12.9
MS_1	Gain(dBi)	18.2	19.1	20.1
	SLL (dB) (*xoz*/*yoz*)	-21.67/-17.2	-30.4/-18.98	-21.23/-19.6
	η_a	43.78%	40.64%	36.8%

significantly reduced compared to MS_0. Especially, the SLLs of MS_1 decrease by 21.2 dB in *xoz*-plane and 6.88 dB in the *yoz*-plane at 16 GHz. Meanwhile, η_a (according to [13]) of MS_1 are 43.78%, 40.64%, and 36.8% at 14, 16, and 19 GHz, respectively. It is noting that the simulated η_a of MS_1 is lower than the calculated one according to [17]. The reasons are as follows. First, η_a in [17] does not include the efficiency factors associated with the feed loss, reflectarray element loss, polarization loss, and mismatch loss. Second, the beam of MS_1 is deflected resulting that the effective aperture is decreased. Therefore, η_a is reduced. Third, compared with the single-beam antenna, the dual-beam antenna has more sidelobes and leads to lower η_a.

Finally, the proposed method is compared with that based on Taylor distribution and results are shown in Fig. 10. From Fig. 10(a), it can be observed that amplitudes from Taylor distribution are tapered along the aperture and are not related to the direction of beam. But for the proposed method, the amplitudes distribute in a complex way and two submaximum

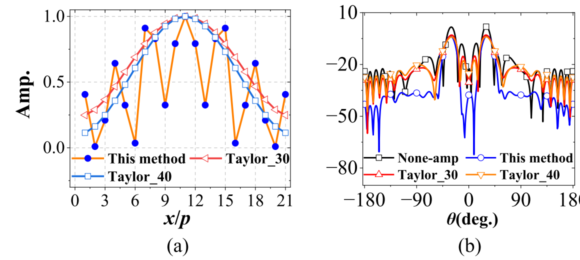

Fig. 10. Comparison results between this method and Taylor distribution. (a) Amplitude distribution. (b) Radiation pattern in the *xoz*-plane. (**Annotation**: "Taylor_M" represents Taylor distribution when the SLL is set to be -M dB.).

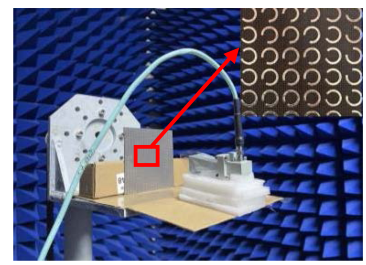

Fig. 11. Photograph of the measurement.

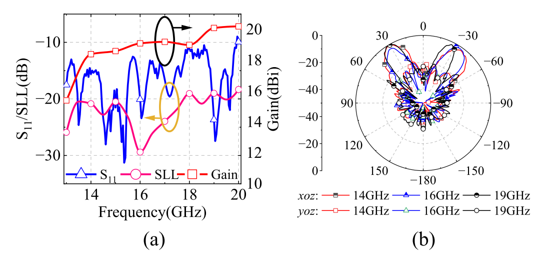

Fig. 12. Measured results of MS_1. (a) S_{11}, SLL, and peak gain. (b) 2-D results in *xoz*-and *yoz*-plane.

values relating with dual beams appear. As a result, this method suppresses the SLL more efficiently than the way based on Taylor distribution as shown in Fig. 10(b).

IV. EXPERIMENT VERIFICATION

To experimentally demonstrate the proposed method, a prototype of MS_1 with a size of 105 mm $\times$ 105 mm is fabricated and measured as shown in Fig. 11, and the measured results are shown in Fig. 12. Fig. 12(a) displays the measured S_{11}, peak gain, and SLL of the MS_1. It indicates that MS_1 can operate from 14 to 19 GHz. In the operating band, the gain increases with frequency and all are larger than 18 dBi. Also, SLLs in the *xoz*-plane are lower than -19 dB. Especially, at 16 GHz, the SLL could reach -29.65 dB, matching the target. Fig. 12(b) shows normalized radiation patterns at 14, 16, and 19 GHz in *xoz*-and *yoz*-plane, which are consistent with the simulated results in Fig. 9(b).

V. CONCLUSION

In this letter, a method of suppressing the SLLs of the dual-beam antenna is proposed. Based on the method, a dual beam antenna with low SLL is designed, fabricated, and measured. The measured results match well with the simulated ones, which verify the effectiveness and reliability of the proposed method.

References

[1] G. Li, Y. Ge, and Z. Chen, "A compact multibeam folded transmitarray antenna at Ku-band," *IEEE Antennas Wireless Propag. Lett.*, vol. 20, no. 5, pp. 808–812, May 2021.

[2] H.-F. Wang, Z.-B. Wang, Z.-H. Wu, and Y.-R. Zhang, "Beam-scanning lens antenna based on elliptical paraboloid phase distribution metasurfaces," *IEEE Antennas Wireless Propag. Lett.*, vol. 18, no. 8, pp. 1562–1566, Aug. 2019.

[3] L.-Z. Song, X. Wang, and P.-Y. Qin, "Single-feed multibeam conformal transmitarrays with phase and amplitude modulations," *IEEE Antennas Wireless Propag. Lett.*, vol. 21, no. 8, pp. 1669–1673, Aug. 2022.

[4] H. Li, G. Wang, J. Liang, X. Gao, H. Hou, and X. Jia, "Single-layer focusing gradient metasurface for ultrathin planar lens antenna application," *IEEE Trans. Antennas Propag.*, vol. 65, no. 3, pp. 1452–1457, Mar. 2017.

[5] H. P. Li, G. M. Wang, T. Cai, J. G. Liang, and X. J. Gao, "Phase- and amplitude-control metasurfaces for antenna main-lobe and side-lobe manipulations," *IEEE Trans. Antennas Propag.*, vol. 66, no. 10, pp. 5121–5129, Oct. 2018.

[6] Q. Lou and Z. N. Chen, "Sidelobe suppression of metalens antenna by amplitude and phase controllable metasurfaces," *IEEE Trans. Antennas Propag.*, vol. 69, no. 10, pp. 6977–6981, Oct. 2021.

[7] R. C. Hansen, *Phased Array Antennas*. Hoboken, NJ, USA: Wiley, 2009.

[8] Y. J. Guo, M. Ansari, R. W. Ziolkowski, and N. J. G. Fonseca, "Quasi-optical multi-beam antenna technologies for B5G and 6G mmWave and THz networks: A review," *IEEE Open J. Antennas Propag.*, vol. no. 2, pp. 807–830, 2021.

[9] Y. J. Guo and R. W. Ziolkowski, *Advanced Antenna Array Engineering for 6G and Beyond Wireless Communications*. Hoboken, NJ, USA: Wiley, 2021.

[10] W. Hong et al., "Multibeam antenna technologies for 5G wireless communications," *IEEE Trans. Antennas Propag.*, vol. 65, no. 12, pp. 6231–6249, Dec. 2017.

[11] C. H. Lee, T. V. Hoang, S. W. Chi, S. G. Lee, and J. H. Lee, "Low profile quad-beam circularly polarised antenna using transmissive metasurface," *Microw., Antennas Propag.*, vol. 13, no. 10, pp. 1690–1698, 2019.

[12] L. Bao et al., "Multi-beam forming and controls by metasurface with phase and amplitude modulations," *IEEE Trans. Antennas Propag.*, vol. 67, no. 10, pp. 6680–6685, Oct. 2019.

[13] P. Nayeri, F. Yang, and A. Z. Elsherbeni, "Design and experiment of a single-feed quad-beam reflectarray antenna," *IEEE Trans. Antennas Propag.*, vol. 60, no. 2, pp. 1166–1171, Feb. 2012.

[14] Y. Hu, W. Hong, and Z. H. Jiang, "A multibeam folded reflectarray antenna with wide coverage and integrated primary sources for millimeter-wave massive MIMO applications," *IEEE Trans. Antennas Propag.*, vol. 66, no. 12, pp. 6875–6882, Dec. 2018.

[15] P. Zhang, L. Li, X. M. Zhang, H. X. Liu, and Y. Shi, "Design, measurement and analysis of near-field focusing reflective metasurface for dual-polarization and multi-focus wireless power transfer," *IEEE Access*, vol. 7, pp. 110387–110399, 2019.

[16] S. Li, Z. N. Chen, T. Li, F. H. Lin, and X. Yin, "Characterization of metasurface lens antenna for sub-6 GHz dual-polarization full-dimension massive MIMO and multibeam systems," *IEEE Trans. Antennas Propag.*, vol. 68, no. 3, pp. 1366–1377, Mar. 2020.

[17] A. Yu, F. Yang, A. Z. Elsherbeni, J. Huang, and Y. Rahmat-Samii, "Aperture efficiency analysis of reflectarray antennas," *Microw. Opt. Technol. Lett.*, vol. 52, no. 2, pp. 364–372, Feb. 2010.

[18] C. A. Balanis, *Antenna Theory: Analysis and Design*. Hoboken, NJ, USA: Wiley, 2016.